Morphological and spatial control of InP growth using closed-space sublimation

Daisuke Kiriya,[1,2,3,a)] Maxwell Zheng,[1,2,3,a)] Rehan Kapadia,[1,2,3] Junjun Zhang,[1,2,3] Mark Hettick,[1,2] Zhibin Yu,[1,2,3] Kuniharu Takei,[1,2,3] Hsin-Hua Hank Wang,[1] Peter Lobaccaro,[1,2] and Ali Javey[1,2,3,b)]
[1]*Electrical Engineering and Computer Sciences, University of California, Berkeley, California 94720, USA*
[2]*Materials Sciences Division, Lawrence Berkeley National Laboratory, Berkeley, California 94720, USA*
[3]*Berkeley Sensor and Actuator Center, University of California, Berkeley, California 94720, USA*

(Received 12 September 2012; accepted 7 November 2012; published online 18 December 2012)

Scalable growth of high quality III-V semiconductor thin films on non-epitaxial substrates is of profound interest for photovoltaic applications. Here, we demonstrate growth of indium phosphide (InP) crystals directly on metal foils using closed-space sublimation (CSS) method. CSS allows effective transfer of source material to the substrate due to a small (~2 mm gap between source and substrate) sublimation space. The crystallization kinetics are found to be dependent on the substrate temperature and pressure of the system. Importantly, experiments revealed that both InP nanowires and polycrystalline films could be obtained by tuning the growth conditions. Furthermore, utilizing a silicon dioxide mask, selective nucleation of InP on metal substrates was obtained. Photoluminescence measurements depict the high optical quality of the CSS grown InP. © *2012 American Institute of Physics*. [http://dx.doi.org/10.1063/1.4768836]

I. INTRODUCTION

III-V semiconductor materials have demonstrated the highest performing photovoltaic (PV) devices in terms of power conversion efficiencies.[1] Indium phosphide (InP) is a good candidate for single junction photovoltaics because it has an ideal band gap[2] and is reported to have low surface recombination velocity (SRV) (~10^3 cm s^{-1})[3–7] compared to the other III-V materials such as gallium arsenide (~10^6 cm s^{-1}).[7,8] For practical applications, however, development of a growth process technique with the following attributes is needed: (i) low fabrication costs and the potential for large-area manufacturing,[2] (ii) spatial control (selective growth) and (iii) crystalline morphology control for application specific tailoring of material properties. Currently, research on metal organic chemical vapor deposition (MOCVD)[9–11] and molecular beam epitaxy (MBE)[12,13] have been primarily used for InP crystal growth, both epitaxially and on metal foils. Specifically, our recent work has shown that non-epitaxially grown InP polycrystalline films on metal foils by MOCVD exhibit near identical optical properties (e.g., photoluminescence (PL) spectra) as InP single-crystal wafer,[11] indicating that polycrystalline InP is a promising material system for high performance PV cells. However, MOCVD and MBE are not suitable for low cost, high throughput manufacturing given their low raw material utilization yields, expensive precursors, and/or slow growth rates.[14–16] Here, we report a scalable growth method for producing InP crystals directly on metal foils that allows both spatial control (e.g., polycrystalline thin film and selective area growth of crystalline arrays) and morphology control (e.g., from nanowires (NWs) to faceted crystals) using the closed-space sublimation (CSS) technique. The CSS technique[17] provides a small precursor transport distance, which allows efficient transfer of source material to the substrate (Figures 1(a) and 1(b). Therefore, CSS provides a high crystalline growth rate and potentially high throughput with minimal source material loss.[18] CSS is a well-established method for making polycrystalline thin-film solar cells, especially for CdTe with the explored device efficiencies of 17.3% (Ref. 19) which highlights its ability to yield high quality crystal growth. In this research, we further reveal that the enclosed space facilitates saturated vapor phases of the source materials, thereby enabling nucleation and growth of high quality InP crystals with promising optical properties as examined by steady-state and time-resolved photoluminescence (TRPL) analyses. Thus CSS growth of InP should be a promising candidate for use in thin film III-V solar cells applications.

II. EXPERIMENTAL DETAILS

A. CSS system and growth procedures

The CSS system used here was built by Engineered Science. The glass chamber size was about 10-in. long and 5-in. diameter. The glass folder held graphite blocks. Inside the graphite blocks precursor, InP powder (99.999%, China Rare Metal Co.) and molybdenum (Mo) foil (99.95%) were sandwiched. The spacer thickness was ~2 mm. The chamber was evacuated and purged with N_2 gas. Growth substrate (T_{sub}) and source (T_{so}) temperatures ranged from $T_{sub} = 485$ to 700 °C and $T_{so} = 650$ to 800 °C, respectively. Growth times explored were 15−60 min and pressure (P) range was 0.1 to 40 Torr. The Mo foils used were 25 μm thick and cleaned with acetone and isopropanol prior to growth.

[a)]D. Kiriya and M. Zheng contributed equally to this work.
[b)]Author to whom correspondence should be addressed. Electronic mail: ajavey@berkeley.edu.

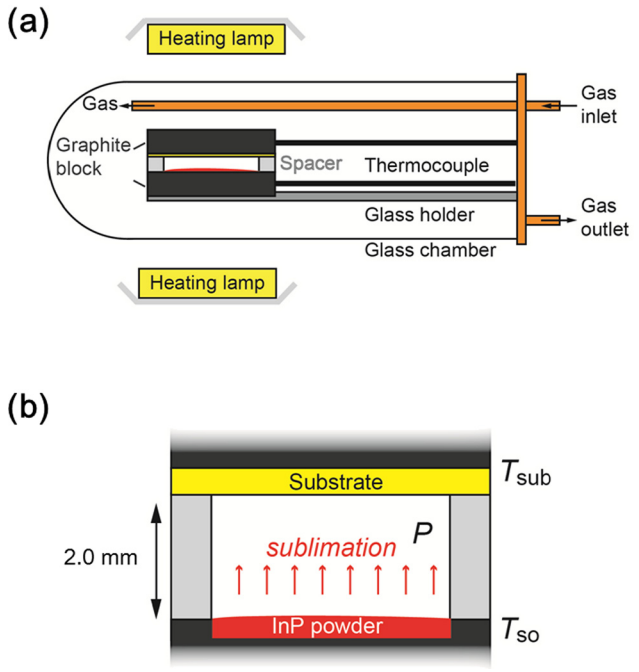

FIG. 1. Schematic illustration of the CSS system. (a) Overview of the CSS instrument. A glass chamber contains two graphite blocks. The substrate and precursor powder are located inside the graphite top and bottom blocks, respectively. Graphite blocks are heated using halogen lamps, while the temperature of the blocks is monitored using thermocouples. Atmosphere of the chamber is exchanged using gas inlet and outlet. Here, we used N_2 gas. Pressure inside the chamber is also controlled by adjusting the N_2 gas flow. (b) An enlarged image of the sublimation component of the chamber. Controlled parameters are substrate temperature (T_{sub}), source InP powder temperature (T_{so}), pressure of the system (P), and growth time.

B. Fabrication of patterned Mo substrates

Mo dots on silicon oxide were fabricated as follows: 50 nm thick, 1.5 μm diameter Mo circles on silicon oxide/silicon wafer were fabricated using a standard lift-off process. The thickness of silicon oxide was 50 nm, and the Mo was deposited via sputtering. The Mo holes were fabricated as follows: 15 nm silicon oxide (SiO_x) was deposited on Mo foil by electron-beam evaporation. A photoresist (PMMA 495 C2) was spin coated (3000 rpm, 1 min) on the Mo foil (25 μm). The foil was baked for 1 min at 180 °C on a hotplate. Acetone was then poured onto a patterned polydimethylsiloxane (PDMS, same dot pattern as shown in Figure 4(a)), and the PDMS put onto the foil for 1 h. The PDMS dot pattern was subsequently transferred to the foil. Finally, the SiO_x was etched using 0.2% hydrofluoric acid, and the photoresist removed by remover-PG.

C. Physical measurements

The X-ray diffraction (XRD) was taken on a Bruker AXS D8 Discover GADDS XRD Diffractometer system. The PL excitation source was a 785 nm laser with ~5 μm spot size, and the detector was a silicon CCD. The TRPL excitation source was a tunable Mira 900-F Ti-sapphire laser set to 800 nm, producing 200 fs pulses at 75.3 MHz. The detector was a Si avalanche photodiode (APD) (id-100) produced by id Quantique hooked up to a Time-Correlated Single Photon Counting (TCSPC) module (SPC-130) from Becker & Hickl. The sample (InP crystals on Mo dots shown in Figure 4(b)) for PL and TRPL measurements was treated by 2 min 1% hydrochloric acid (HCl) and 2 min 15% nitric acid (HNO_3) in advance. These treatments removed surface oxides and passivated the InP crystals.[20,21] Scanning electron microscope (SEM) images were taken on a Zeiss Gemini Ultra-55 and JEOL 6340F. The Mott-Schottky measurements were performed with a SP-300 Potentiostat set-up (BioLogic, France) for the InP polycrystalline film ($T_{sub} = 600$ °C (15 min), 680 °C (30 min) then 600 °C (15 min), $T_{so} = 800$ °C, $P = 0.2$ Torr) in 3.0 M potassium chloride (KCl) solution. Before the measurement, the InP polycrystalline film was transferred to a glass substrate by peeling it off from the Mo foil using glue. The InP polycrystalline film was covered by a glue (Advanced Formula Instant Krazy Glue, Elmer's Products, Inc), then lifted off from the Mo foil after curing of the glue. The sample was etched before the measurement by 1 M HCl for 2 min to remove any residual molybdenum phosphide (MoP) that may have peeled off. Mott–Schottky plots of these data are shown in Figure S9 for different frequencies. The potential scan started at −0.4 V down to 0.2 V with steps of 20 mV. The frequency range was 99 Hz to 80 kHz. The carrier concentration was calculated from the slope of the $1/C_2$ vs potential plot, where C is the capacitance of the space charge layer. According to the frequency dispersion data (Figure S9b), the free electron concentration was 0.8–4.6 × 10^{18} cm^{-3}.

III. RESULTS AND DISCUSSION

Figure 1(a) illustrates an overview of the CSS system. It includes two graphite blocks encapsulated in a glass chamber. The top and bottom graphite blocks partially enclose a substrate and the InP source powder, respectively, and these are separated by a spacer (thickness ~2 mm). The temperature of each graphite block is controlled by separate halogen lamps and monitored by separate thermocouples. The important parameters in a CSS system are (i) the temperatures of the source material (T_{so}) and the growth substrate (T_{sub}), (ii) chamber pressure (P), (iii) and growth time (Figure 1(b)). Thus, these parameters were explored to optimize the growth conditions. Additionally, proper substrate choice is critical. Here, Mo foil is chosen due to (i) a lack of any In-Mo intermetallics up to the growth temperature and (ii) low solubility of In in Mo at the growth temperature.[11] Additionally, the thermal coefficient of Mo is similar to InP.[22] By sublimation of InP powder, polycrystalline InP was grown on Mo foil as illustrated in Figure 2(a). From visual inspection, the grown InP films exhibited large area (2 cm × 2 cm) uniformity (Figure 2(b)). Figures 2(c) and 2(d) show the top- and side-view SEM images of a representative polycrystalline InP thin film (~7 μm thickness) grown on Mo foil. The average grain size for this growth condition is ~5 μm. The crystalline size and morphology are highly dependent on the growth condition (*vide infra*) and the most continuous polycrystalline film was obtained using $T_{sub} = 600$ °C (15 min), 680 °C (30 min), then 600 °C (15 min) and $T_{so} = 800$ °C and $P = 0.2$ Torr in the growth procedure (Figures 2(c) and 2(d)). The initial lower temperature growth ($T_{sub} = 600$ °C) is used to promote uniform nucleation of InP, enabling continuous film growth,

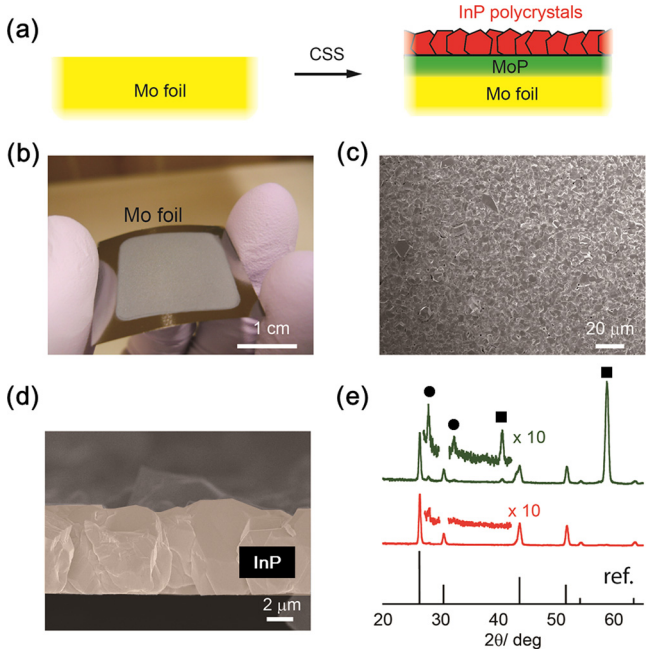

FIG. 2. Polycrystalline InP growth on a Mo foil. (a) Illustrative image before (left) and after (right) the growth of a polycrystalline InP film on a Mo foil. (b) Macroscopic picture of uniform InP polycrystalline film fabricated on a Mo foil. (c) SEM image of the InP polycrystalline film growth with the condition of (T_{sub} = 600 °C (15 min), 680 °C (30 min) then 600 °C (15 min), T_{so} = 800 °C, P = 0.2 Torr). The crystalline size is 5–7 μm. (d) Cross-sectional SEM image of a free-standing InP polycrystalline film which delaminated after cutting the foil. The film thickness is estimated to be ~7 μm. (e) XRD patterns for InP crystals. Curves are normalized to the (111) peak of InP (2 θ = 26.3°) and offset. (Top) dispersed InP crystals fabricated on Mo foil (T_{sub} = 700 °C, T_{so} = 750 °C, P = 1 Torr, 30 min growth). (110) and (200) of Mo peaks (■) and (001) and (100) of MoP peaks (•) were labeled. (Middle) InP polycrystalline continuous film on a Mo foil (T_{sub} = 685 °C, T_{so} = 800 °C, P = 1 Torr, 30 min growth). (Bottom) reference peaks of InP from International Centre for Diffraction Data (ICDD) Powder Diffraction File (PDF). From left to right, the InP peaks are as follows: (111), (200), (220), (311), (222), and (400).

while the higher temperature growth (T_{sub} = 680 °C) is used to promote larger grain sizes. The final low temperature step is necessary to minimize pinholes in the film. XRD characterization shows the InP crystalline peaks (Figure 2(e)) match those of zincblende InP.[11,23] No preferential orientation was observed. By reducing the source temperature, lower flux growth conditions (e.g., T_{sub} = 700 °C, T_{so} = 750 °C, P = 1 Torr, and 30 min growth) were obtained with low surface coverage of InP crystals on the substrate. From the resulting samples, both Mo and MoP peaks[24,25] were observed. This result is consistent with the previous InP growth using MOCVD.[11] Note that from our previous study of InP MOCVD growth on Mo, a self-limiting thin layer (~50 nm thickness) of MoP is found to form at the Mo/InP interface during the growth. Here, the Mo surface is also phosphorized during the CSS growth as illustrated in Figure 2(a). We note here that the use of flexible metal foil substrates is attractive given its compatibility with large-scale industrial processes such as roll-to-roll fabrication.

Mott-Schottky measurements were performed to characterize the carrier concentration of the CSS grown InP films. The results indicate that the grown InP is n-type, with an electron carrier concentration in the range of ~0.8–4.6×10^{18} cm^{-3} (see Supporting Information for measurement details[35]). This relatively high electron concentration could be due to carbon incorporation[26] from the graphite blocks used in the set-up or phosphorous vacancies near the surface, both of which are known to be donors in InP. These unintentional doping sources can be mitigated in the future by coating the graphite blocks with an inert material and/or by mixing in additional phosphorous to the source InP powder. It is also possible for impurities in the source powder to cause doping.

Additionally, the temperature and pressure dependency of InP structures were systematically explored. The morphology of the InP crystals as shown in Figure 3 is highly dependent on T_{sub} and P. Specifically, in the range of T_{sub} between 485 °C to 650 °C with P greater than 1 Torr, we obtained self-catalyzed InP NWs. The NW morphologies can be categorized into two types depending on the conditions: (i) NWs with In-rich tips and (ii) NWs without tips. The vapor-liquid-solid (VLS) growth mechanism[27] is well established for NW growth, and it appears the NWs with In-rich tips grow via a VLS mechanism, where an indium droplet first forms on the substrate, followed by absorption of phosphorous from the environment and finally precipitation of InP. On the other hand, the NWs without tips are observed at higher temperatures (above 500 °C). This morphology suggests that both VLS and vapor-solid-solid (VSS) mechanisms are at work. This agrees well with previous reports of NWs fabricated by metal organic vapor phase epitaxy.[27] At higher temperature (T_{sub} > 650 °C and P > 1 Torr), we obtained faceted (polycrystalline) InP crystals as shown in Figures 2(c) and 2(d), and S4-S6. Though not exhaustive, this study clearly shows CSS can controllably produce morphologies ranging from NWs to polycrystalline films by varying the growth conditions. Therefore, application-specific structures can be engineered. For example, water-splitting and catalysis may benefit from the NW structures[28] because of the large surface area, while faceted crystals may be better for fabricating high efficiency solar cells.

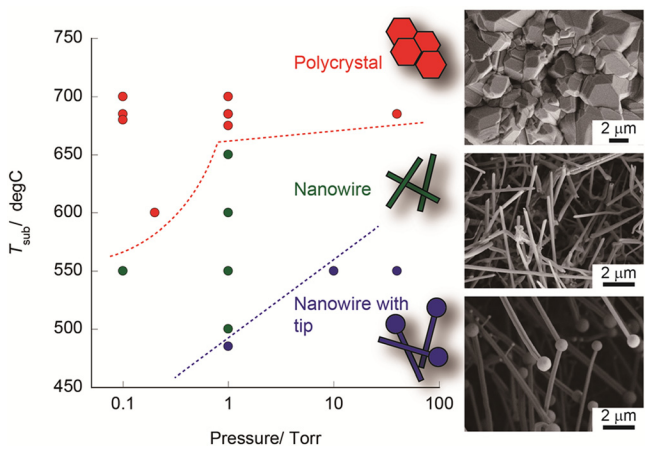

FIG. 3. Temperature (T_{sub}) – pressure (P) dependence of the InP morphologies grown by CSS. The SEM images from top to bottom are as followed: polycrystalline film (T_{sub} = 685 °C, T_{so} = 800 °C, P = 1 Torr, 30 min growth), nanowires (T_{sub} = 550 °C, T_{so} = 700 °C, P = 0.1 Torr, 30 min growth), and nanowires with In-rich tips (T_{sub} = 550 °C, T_{so} = 700 °C, P = 10 Torr, 30 min growth). Scale bars are 2 μm.

Next the time dependence of the CSS InP growth mechanism was studied. 30 min and 60 min growths were performed with all other conditions held constant ($T_{sub} = 685\,^{\circ}C$, $T_{so} = 800\,^{\circ}C$, $P = 0.1$ Torr, and 0.5 g InP source). Figure S1 shows the results for 60 min sublimation time; silver-colored In bumps were obtained on the Mo foil without InP. On the other hand, the 30 min growth at the same conditions produced the InP crystalline phase (Figure 2(e) and S5). These results enable postulation of the CSS growth mechanism (Figure S1). During the initial sublimation processes (Figure S1c steps 1 to 2), both indium and phosphorous sublimate resulting in a net flux towards the substrate and InP crystals growth. Given the higher vapor pressure of P as compared to In, after some time (step 3), further annealing leads to a net phosphorous loss from the chamber, causing the InP crystals on the substrate to decompose (step 4). Eventually, indium bumps on Mo foil are obtained (step 5) if the samples are heated for too long. We note that we kept T_{sub} the same in all steps 1 to 5, revealing that $T_{sub} = 685\,^{\circ}C$ is high enough to decompose InP. Therefore, the InP crystals are grown at higher temperature than their decomposition temperature; this indicates that both phosphorous and indium are "super-saturated" during the growth process when the growth time is not too long. This super-saturation pushes the equilibrium shown in Eq. (1)[29] towards formation of InP crystals.

$$\mathrm{InP}(solid) \rightleftarrows \mathrm{In}(liquid/gas) + 1/4\mathrm{P_4}(gas). \qquad (1)$$

The super-saturated environment, facilitated by the confined space in a CSS system, also enables us to operate above the disassociation temperature. Therefore, crystals are synthesized at a higher temperature, which potentially allows the growth of higher quality crystals.

Spatial control of the crystalline growth is important for a variety of applications. Primarily, for solar cells, the benefits include reducing grain boundaries[30] which act as recombination centers and shunt paths.[30,31] In this context, we examined the selective growth of InP crystals using the CSS technique. Two types of substrates were examined by patterning Mo with a silicon oxide masking layer as shown in Figure 4. In the first type of sample, Mo holes (1.5 μm diameter) are made by depositing a 15 nm SiO_x layer via electron beam evaporation on a Mo foil, followed by patterned etching of SiO_x. InP growth only occurred on the Mo holes; each crystal (about 5 μm diameter) sat on the Mo holes without any InP nucleation on the SiO_x surface (Figures 4(a) and S7). The reason for this is that InP growth is strongly inhibited on silicon oxide surfaces.[13] In the second type of substrate, 50 nm thick sputtered Mo dots (1.5 μm diameter) were patterned on a silicon oxide/silicon wafer (thermal oxide, 50 nm thickness) using traditional photolithography and lift-off processes. 5 to 7 μm InP crystals were then selectively grown on the Mo dots. The InP crystals are separate from each other and nearly all look like single crystals, which can be seen from a cross-sectional SEM view (Figure S8). Each crystal was about 7 μm in height. As demonstrated here, selective area growth of InP crystals on both Mo holes and dots is possible, which can facilitate the use of CSS for making precise optoelectronic devices.

We further analyzed the optoelectronic properties of InP crystals. Room temperature steady-state PL spectra (Figure 5(a)) of InP crystals on Mo dots show an asymmetric feature with the peak at ~1.34 eV. Compared to an $8 \times 10^{15}\,cm^{-3}$ *n*-type InP single-crystal wafer, the peak position is nearly the same and the full-width-at-half-maximum (FWHM) is slightly broader (0.060 eV vs. 0.045 eV). This result shows the high optical quality of our CSS grown InP. The slight peak broadening can be explained by a higher carrier concentration in our material,[32] which is corroborated by the doping levels ($0.8–4.6 \times 10^{18}\,cm^{-3}$) extracted from Mott-Schottky measurements on thin films (Figure S9). To further analyze the quality of the crystals from the underlying recombination processes, a study of the photoluminescence intensity as a function of incident laser power was performed (Figure 5(b)). The result suggests that exciton recombination dominates. This relationship can be seen in a log-log plot, for which the relation is given by $I_{PL} = CI_L^{\,k}$, where I_{PL} is the PL intensity, I_L is the illumination power, C is a proportionality constant, and k is the power dependence of the PL

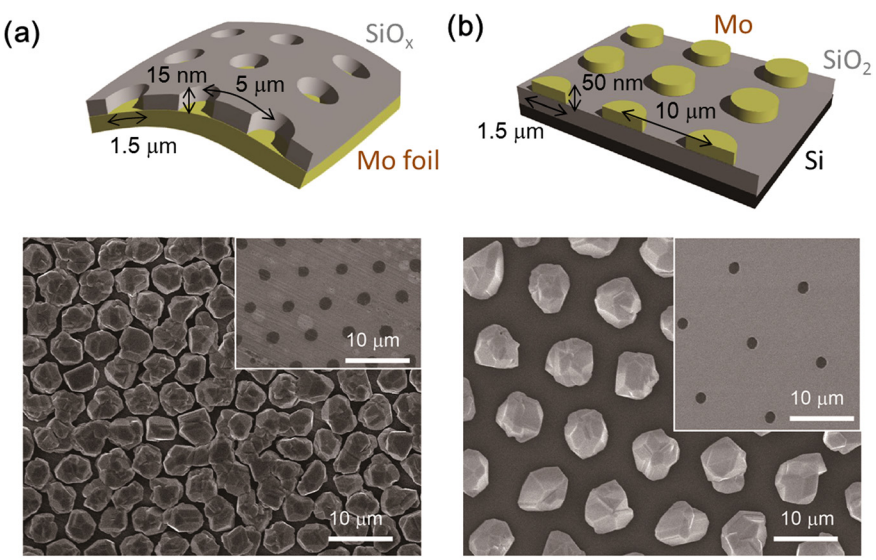

FIG. 4. Spatial control of InP crystal growth. (a) (Top) illustrative image of Mo holes on the foil covered with silicon oxide. (Bottom) SEM images of the InP crystal growth on the Mo holes and (Inset) the patterned foil before the CSS growth. (b) (Top) illustrative image of Mo dots on a silicon substrate covered with silicon oxide. (Bottom) SEM images of the InP crystal growth on the Mo dots and (inset) the patterned substrate before the CSS growth. Scale bars are 10 μm.

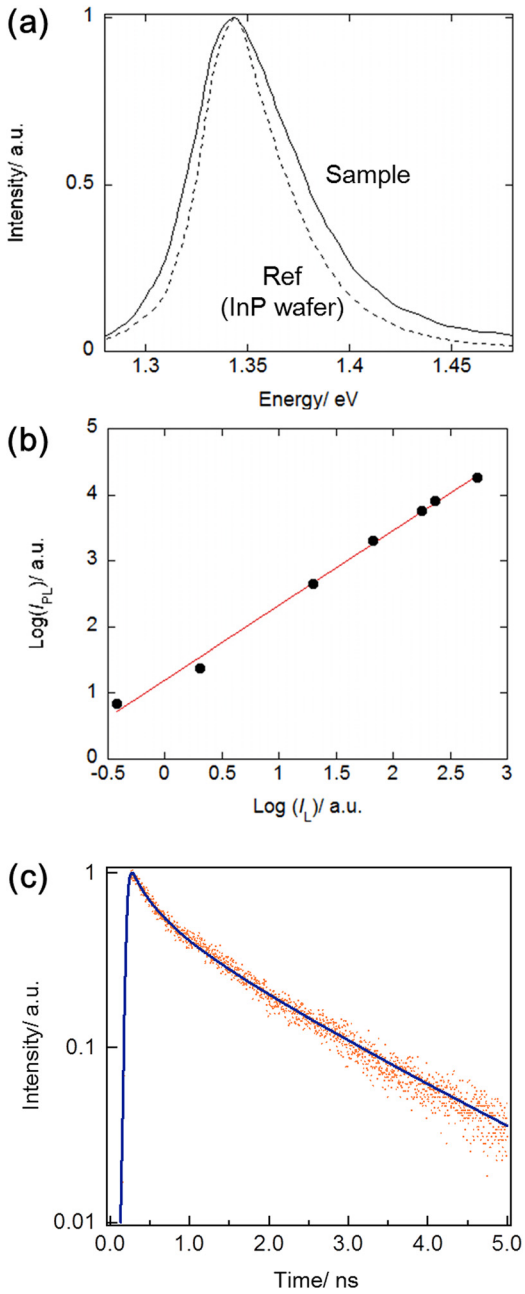

FIG. 5. Optical properties of the InP crystals on the Mo dots. (a) PL spectra of CSS grown InP sample (solid line) and an InP reference wafer (dashed line, electron concentration is $8 \times 10^{15}\,cm^{-3}$). (b) Laser power ($I_L$) vs. PL intensity ($I_{PL}$) plot. The red line is a linear fit with a slope of ~1.13. (c) TRPL plot and the simulated curve (solid line) of the InP crystals on Mo dots. The sample was treated by 2 min 1% HCl and 2 min 15% HNO_3 in advance.

intensity.[33] For a direct band gap material, a value of $k < 1$ is expected for free-to-bound recombination (electron to acceptor or hole to donor), $k = 1$ is expected for free or bound exciton recombination, and $k = 2$ is expected when defect state recombination dominates.[33] We find $k = 1.13 \pm 0.03$ by a linear fit to the log-log plot. This result provides additional evidence for a high optical quality film, as the close value of $k \sim 1$ indicates defect (nonradiative) recombination is not significant.

To determine the carrier lifetime, TRPL measurements were carried out for the InP crystals on Mo dots (Figure 5(c)). The sample was illuminated with 800 nm incident light at an illumination power of $P_0 = 440$ mW and a spot size of $A = \pi * 200^2\,\mu m^2$, giving an excess carrier concentration of $\sim 6 \times 10^{17}\,cm^{-3}$ at the surface; the generation rate is given by $G = \alpha * P_0/(E_{ph} * A)$, where absorption coefficient $(\alpha) = 3.37 \times 10^4\,cm^{-1}$, and the photon energy $(E^{ph}) = 1.55$ eV. The TRPL decay time (1/e) of our sample is 0.89 ns. The previously reported TRPL decay time in an InP single-crystalline film grown by the liquid phase epitaxial process is 0.94 ns for the doping concentration of $5.3 \times 10^{18}\,cm^{-3}$.[34] This provides further evidence that the CSS grown crystals have a similar optical quality as the InP single crystalline wafers.

Furthermore, the diffusion equation was solved to simulate a TRPL decay curve. The fitting parameters were bulk recombination lifetime (τ) and effective SRV at the top surface. Due to the thickness of the sample (~7 μm), the lifetime was insensitive to back surface recombination, which was therefore not considered. The simulated decay curve was then convolved with the measured instrument response and fit to the experimentally measured curve (Figure 5(c)). Using an ambipolar diffusion coefficient of 5.2 $cm^2\,s^{-1}$ and a bulk electron concentration of $3 \times 10^{18}\,cm^{-3}$, τ and effective SRV were extracted to be 3.0 ns and $1.9 \times 10^5\,cm\,s^{-1}$, respectively. This SRV value is higher than previous TRPL results for *n*-type InP;[3–7] however, it should be possible to reduce this with appropriate surface treatment. It should be noted that the ambipolar diffusion coefficient was calculated using electron and hole mobilities of single crystalline InP for the same carrier concentration. In the future, detailed Hall effect measurements need to be performed to more directly assess the diffusion coefficients and thereby the carrier lifetimes. TRPL studies on single crystal *n*-InP with similar concentrations have not extracted the bulk recombination time in the past.

IV. CONCLUSIONS

We have demonstrated morphology and spatial control of InP grown on Mo foils using the CSS technique. The crystals grown using this technique are composed of micron-sized grains and show respectable carrier lifetimes as measured by TRPL characterization. The confined space of CSS produces supersaturation of the source gases enabling growth at higher temperatures, which promotes high optical quality InP crystals. In the future, further characterization of the minority carrier lifetime, mobility, and diffusion lengths are needed. Appropriate dopants, substrates, and surface modifications will also need to be explored for making high quality opto-electronic devices. This simple growth scheme relies only on sublimation of a solid powder inside the growth chamber, removing the need for expensive systems and single-crystalline substrates, which are limiting factors in the current III-V growth technologies for low-cost devices. The use of metal foil substrates is important to not only reduce cost at the material growth step but also at the downstream processing steps given its mechanical properties. Consequently, CSS grown InP shows high promise for high-efficiency and low-cost solar cells.

ACKNOWLEDGMENTS

This work was supported by the Director, Office of Science, Office of Basic Energy Sciences, Materials Sciences, and Engineering Division of the U.S. Department of Energy under Contract No. DE-AC02-05CH11231. A.J. acknowledges support from the World Class University program at Sunchon National University, and DOE funded Bay Area PV Consortium. D.K. is grateful for a JSPS Postdoctoral Fellowship for Research Abroad.

[1]M. A. Green, K. Emery, Y. Hishikawa, W. Warta, and E. E. Dunlop, Prog. Photovoltaics **20**, 12 (2012).
[2]R. W. Miles, G. Zoppi, and I. Forbes, Mater. Today **10**, 20 (2007).
[3]T. Nakamura and T. Katoda, J. Appl. Phys. **55**, 3064 (1984).
[4]Y. Rosenwaks, Y. Shapira, and D. Huppert, Phys. Rev. B **44**, 13097 (1991).
[5]Y. Rosenwaks, Y. Shapira, and D. Huppert, Phys. Rev. B **45**, 9108 (1992).
[6]S. Bothra, S. Tyagi, S. K. Ghandhi, and J. M. Borrego, Solid-State Electron. **34**, 47 (1991).
[7]D. D. Nolte, Solid-State Electron. **33**, 295 (1990).
[8]L. Jastrzebski, J. Lagowski, and H. C. Gatos, Appl. Phys. Lett. **27**, 537 (1975).
[9]T. Saitoh, S. Matsubara, and S. Minagawa, J. Electrochem. Soc. **123**, 403 (1976).
[10]T. Saitoh, S. Matsubara, and S. Minagawa, Jpn. J. Appl. Phys **16**, 807 (1977).
[11]M. Zheng, Z. Yu, T. J. Seok, Y.-Z. Chen, R. Kapadia, K. Takei, S. Aloni, J. W. Ager, M. Wu, Y.-L. Chueh, and A. Javey, J. Appl. Phys. **111**, 123112 (2012).
[12]W. T. Tsang, Appl. Phys. Lett. **45**, 1234 (1984).
[13]K. Araki, J. U. Seo, S. Hasegawa, and H. Asahi, Phys. Status Solidi C **9**, 2766 (2008).
[14]M. Bosi and C. Pelosi, Prog. Photovoltaics **15**, 51–68 (2007).
[15]M. Yamaguchi, T. Takamoto, K. Araki, and N. Ekins-Daukes, Sol. Energy **79**, 78–85 (2005).
[16]G. B. Stringfellow, *Organometallic Vapor-Phase Epitaxy, Theory and Practice*, 2nd ed. (Academic, Boston, 1999).
[17]F. H. Nicoll, J. Electrochem. Soc. **110**, 1165 (1963).
[18]J. Mimila-Arroyo, J. Diaz, A. Lusson, C. Grattepain, R. Bisaro, and J. C. Bourgoin, Mater. Sci. Technol. **12**, 178 (1996).
[19]First Solar, http://investor.firstsolar.com/releasedetail.cfm?ReleaseID=593994, July 26, 2011.
[20]S. K. Krawczyk and G. Hollinger, Appl. Phys. Lett. **45**, 870 (1984).
[21]P. A. Bertrand, J. Vac. Sci. Technol. **18**, 28 (1981).
[22]K. J. Bachmann, E. Buehler, J. L. Shay, and S. Wagner, Appl. Phys. Lett. **29**, 121 (1976).
[23]ICDD PDF-2, Entry 00-032-0452, 2003.
[24]ICDD PDF-2, Entry 00-065-6024, 2003.
[25]ICDD PDF-2, Entry 00-089-5156, 2003.
[26]W. K. Lilu, D. I. Lubyshev, P. Specht, R. Zhao, E. R. Weber, J. Gebauer, A. J. SpringThorpe, R. W. Streater, S. Vijarnwannaluk, W. Songprakob, and R. Zallen, J. Vac. Sci. Technol. B **18**, 1594 (2000).
[27]R. L. Woo, L. Gao, N. Goel, M. K. Hudait, K. L. Wang, S. Kodambaka, and R. F. Hicks, Nano Lett. **9**, 2207 (2009).
[28]M. H. Lee, K. Takei, J. Zhang, R. Kapadia, M. Zheng, Y.-Z. Chen, J. Nah, T. S. Matthews, Y.-L. Chueh, J. W. Ager, and A. Javey, Angew. Chem., Int. Ed. **124**, 10918 (2012).
[29]K. Weiser, J. Phys. Chem. **61**, 513 (1957).
[30]D. Zubía, C. López, M. Rodríguez, A. Escobedo, S. Oyer, L. Romo, S. Rogers, S. Quiñónez, and J. McClure, J. Electron. Mater. **36**, 1599 (2007).
[31]P. N. Gibson, M. A. Baker, E. D. Dunlop, M. E. Özsan, D. Lincot, M. Froment, and G. Agostinelli, Thin Solid Films **387**, 92 (2001).
[32]M. Bugaiski and W. Lewandowski, J. Appl. Phys. **57**, 521 (1985).
[33]T. Schmidt, K. Lischka, and W. Zulehner, Phys. Rev. B **45**, 8989 (1992).
[34]G. Augustine, B. M. Keyes, N. M. Jokerst, A. Rohatgi, and R. K. Ahrenkiel, in *Proceedings of the 5th International Conference on Indium Phosphide Related Materials* (IEEE, 1993), pp. 636–639.
[35]See supplementary material at http://dx.doi.org/10.1063/1.4768836 for the growth mechanism, SEM images of variable conditions, and Mott-Schottky results.